Influence of aorta extracellular matrix in electrospun polycaprolactone scaffolds

JOURNAL OF Applied Polymer SCIENCE

Influence of aorta extracellular matrix in electrospun polycaprolactone scaffolds

James A. Reid, Anthony Callanan
Institute for Bioengineering, School of Engineering, The University of Edinburgh, Edinburgh, United Kingdom
Correspondence to: A. Callanan (E-mail: anthony.callanan@ed.ac.uk)

ABSTRACT: Cardiovascular disease is the leading cause of mortality worldwide. Therefore, new research strategies for the treatment of cardiovascular disease are required. Previously, extracellular matrices (ECMs) have been used alongside polymers to generate hybrid bioscaffolds. Herein, we propose combining aortic ECMs with a polycaprolactone electrospun scaffold and biomechanically evaluating the scaffolds. We electrospun three scaffolds with varying ECM concentrations and found that increasing the ECM concentration leads to decreased stiffness at low strains, increased elasticity at high strain, reduction in failure strain, and an increase in yield strength. We also noted a decrease in water droplet contact angle with the increasing ECM concentration. Furthermore, we found that all three scaffolds were capable of maintaining human umbilical vein endothelial cell attachment and survival. These findings show the wide spectrum of mechanical properties that can be achieved through the addition of different concentrations of ECM into the fibers. © 2019 The Authors. *Journal of Applied Polymer Science* published by Wiley Periodicals, Inc. J. Appl. Polym. Sci. **2019**, *136*, 48181.

KEYWORDS: decellularization; electrospinning; extracellular matrix; polycaprolactone; tissue engineering; vascular

Received 14 November 2018; accepted 5 June 2019
DOI: 10.1002/app.48181

INTRODUCTION

Cardiovascular disease (CVD) is Europe's biggest killer, causing 3.9 million deaths in 2017, accounting for 45% of all deaths.[1] Furthermore, over 85 million people were living with CVD in Europe, leading to an estimated annual economic cost of €210 billion to the European Union alone.[1] Due to the high prevalence and huge socioeconomic burden caused by CVD, the demand for novel treatments is increasing.

There are currently a variety of strategies for the treatment of vascular disease (a subset of CVD focusing on the vessels), including extracellular matrix (ECM) mimicking structures, the use of native ECM components, and functionalized protein laden scaffolds.[2–5] Combining ECM with polymers to manufacture electrospun bioscaffolds has previously been utilized to harness the repeatable mechanical properties of the polymer with the biochemical and mechanical properties of the ECM.[5–8] Electrospinning polymers produces a network of fibers that can be heavily tailored depending on the properties desired.[9] They can be designed to have isotropic or anisotropic mechanical properties, along with three-dimensional architectural properties that favor cell survival and growth.[10] It is possible through electrospinning to include bioactive cues into a repeatable polymer structure and alter its mechanical and physical properties.[5–7,11] This has huge implications in tissue engineering where mimicking the physical and biological properties of the native ECM are major research focusses, especially when the final aim is generation of new functional tissue.

Previous studies have shown that including ECM or ECM proteins into an electrospun polymer scaffold alters its mechanical properties and positively affects seeded cells.[5–7,12] Therefore, in this study, we propose electrospinning a combination of aortic ECM with polycaprolactone (PCL) at two different ECM concentrations and biomechanically evaluating the resulting fibrous scaffolds along with a conventional PCL-only scaffold. Aortic ECM has been chosen as we are looking at a novel solution for the treatment of vascular disease, and therefore have decided to use a type of native ECM directly from a vascular source.

EXPERIMENTAL

ECM Production

Bovine aorta was harvested from a 2 year old female cow. Samples were frozen within 4 h of harvesting at −80 °C and stored until required. A 40 mm diameter sample from the aortic arch was cut out, and all connective tissue was removed after cleaning with ethanol and bathing in water for 30 min to remove blood. A 2 mm punch was used to punch out pieces of aorta for decellularization. The pieces were placed in a decellularizing device and perfusion decellularized with 0.5% w/v sodium dodecyl sulfate (SDS) in diH_2O for 36 h as previously described.[13] Aorta samples were then

perfused with 20 L of diH_2O at 170 mL/min to remove remnant SDS. Samples were frozen and lyophilized in a FreeZone 4.5 freeze-drier (Labconco). Dry ECM was then milled in a plenary ball mill PM 100 (Retsch). ECM powder was then collected and stored at 4 °C for use in electrospinning.

Electrospinning

Powdered ECM was dissolved at either 0.25% w/v or 1% w/v into hexafluoroisopropanol (HFIP) (Manchester Organics). PCL (Mn = 80,000, Sigma Aldrich) was then added to the solutions at 8% w/v and dissolved with agitation. PCL-only scaffolds were used as controls. Solutions were then placed into a 20 mL syringe and pumped using an EP-H11 syringe pump (Harvard Apparatus) into an EC-DIG electrospinning system (IME Technologies). The parameters used were based upon a previously described method: 0.4 mm needle, 0.8 mL/h, 12 cm, +14 kV, −4 kV, 250 RPM.[10] Electrospun fibers were collected onto aluminum foil on a rotating mandrel (diameter = 8 cm) and stored at 4 °C. Scaffolds used with cells were sterilized for 10 min using 70% v/v ethanol. A schematic representation of the decellularizing and electrospinning processes can be seen in Figure 1. These electrospinning solutions lead to final fiber PCL:ECM ratios of 100:0 (PCL only), 96.875:3.125 (0.25% ECM), and 87.5:12.5 (1% ECM).

Scanning Electron Microscopy

Scaffolds were visualized using a Hitachi S4700 fueled emission scanning electron microscope (SEM; Hitachi) with a 5 kV accelerating voltage and a 12 mm working distance. Prior to imaging, all scaffolds were sputter coated with an Emscope SC500A splutter coating using gold–palladium at a ratio of 60:40. Cell seeded scaffolds were visualized after 6 days using a previously described osmium-based method.[8]

Fiber Properties

Scanning electron images were analyzed using ImageJ software (NIH). Briefly, SEM images of the scaffolds were used with fiber diameter being deduced using the DiameterJ plugin and fiber orientation using the OrientationJ plugin.[14] A total of 58 fibers were used to measure fiber diameter and fiber orientation.

Hematoxylin and Eosin Staining

Native and decellularized samples of aorta were fixed in 10% formalin overnight. This was followed by a series of dehydration ranging from 50 to 100% ethanol. Samples were washed in xylene prior to embedding in paraffin wax and were then stored at 4 °C. Samples were trimmed to 5 μm thicknesses and mounted onto slides for hematoxylin and eosin (H&E) staining. Samples then cleared with xylene and mounted in DPX.

Mechanical Testing

Tensile properties were measured using an Instron 3367 testing machine (Instron) with a 50 N load cell. Briefly, 40 mm × 10 mm strips of scaffold were cut and were stretched with a starting gauge length of 20 mm. Scaffolds were stretched to failure at 10 mm/min. Scaffold width was measured using calipers and scaffold thickness measured using a DMK 41 AU02 monochrome 1280 × 960 camera. Incremental Young's modulus was calculated using the formula

$$E_{\text{incremental}} = \frac{\sigma}{\varepsilon} = \frac{FL_0}{A\Delta L} \quad (1)$$

where $E_{\text{incremental}}$ is Young's modulus between two strain bands, σ is stress, ε is strain, F is the applied force, A is the cross-sectional area, ΔL is change in length, and L_0 is the original length. Young's moduli for each scaffold were analyzed and expressed at regular incremental intervals, as previously described.[15–19] Compliance was calculated using following equation

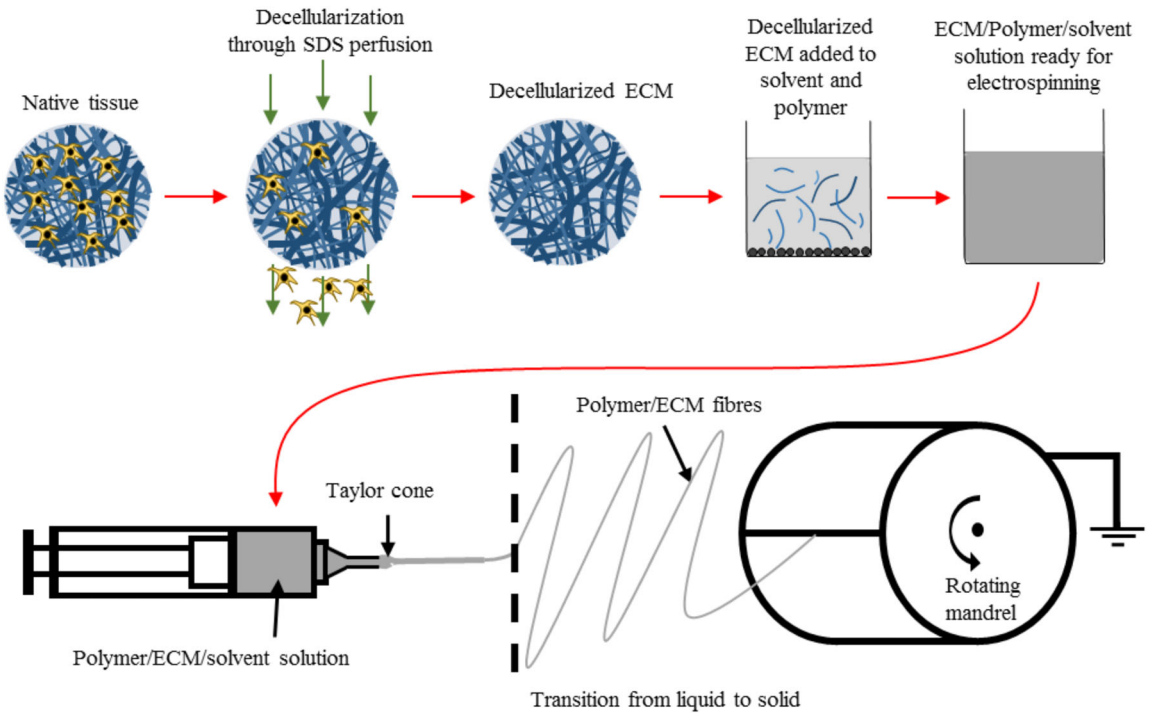

Figure 1. Schematic of the decellularization and electrospinning process. [Color figure can be viewed at wileyonlinelibrary.com]

$$C = \frac{\Delta V}{\Delta P} = \frac{V_1 - V_2}{P_1 - P_2} \quad (2)$$

where V_1 and V_2 are volumes at 0 and 5% strain and P_1 and P_2 are pressures at 0 and 5% strain. Values for ΔP and ΔV between 0 and 5% strain were deduced from thin-wall pressure vessel theory. Briefly, the equation for circumferential stress was reorganized to give us an equation that told us the representative pressure (P_n) at a given stress value σ_n (subscript n denoting that the value is at n% strain).

$$\sigma_n = \frac{P_n d_n}{2t} \quad (3)$$

$$P_n = \frac{\sigma_n \times 2t}{d_n} \quad (4)$$

where σ_n is stress, d_n is the diameter of the representative cylinder, and t is the thickness of the scaffold. Representative volume (V_n) was calculated by treating the strip of scaffold as a cylinder and the strain as a volume increase to this cylinder (subscript n denoting that the value is at n% strain)

$$V_n = \pi \times \left(\frac{d_n}{2}\right)^2 \times w \quad (5)$$

where d_n is the diameter of the representative cylinder and w is the width of the scaffold. For each condition group, $n = 5$.

Contact Angle Measurement

Contact angle was measured on dry scaffolds. A 5 µL droplet of water was placed onto the scaffold, and images were captured using a DMK 41 AU02 monochrome camera at a frequency of 5 Hz. Analysis of the scaffolds was done on ImageJ (NIH) using the LBADSA plugin, as seen in Figure 2.[20]

Cell Culture and Scaffold Seeding

Human umbilical vein endothelial cells (HUVECs) from an infant male Caucasian donor were obtained cryopreserved at passage 1 (Pro-moCell GmbH) and expanded to passage 7 in a 5% CO_2/37 °C atmosphere. HUVECs were expanded using MCBD 131 medium (Life Technologies) supplemented with 5% v/v fetal bovine serum (ThermoFisher Scientific), 1% v/v L-glutamine, 1% v/v penicillin/streptomycin (Life Technologies), 1 mg/L hydrocortisone, 50 mg/L ascorbic acid (Sigma), 2 µg/L fibroblast growth factor (PeproTech), 10 µg/L epidermal growth factor (PeproTech), 2 µg/L insulin-like growth factor (PeproTech), and 1 µg/L VEGF (PeproTech). HUVECs were lifted for scaffold seeding at 80% confluence. Scaffolds (10 mm diameter) were punched out of the electrospun sheet, sterilized in 70% ethanol, and then placed into 48-well plates and soaked in serum free MCDB 131 medium overnight. Wetting medium was removed and scaffolds were then seeded at a density of 350,000 cells/cm^2. Briefly, cells were drip seeded in 30 µL of medium onto the middle of the scaffold. After 30 min, a further 20 µL of medium was added to stop the cells from drying out. After a further 30 min, medium in each well was topped up to 500 µL.

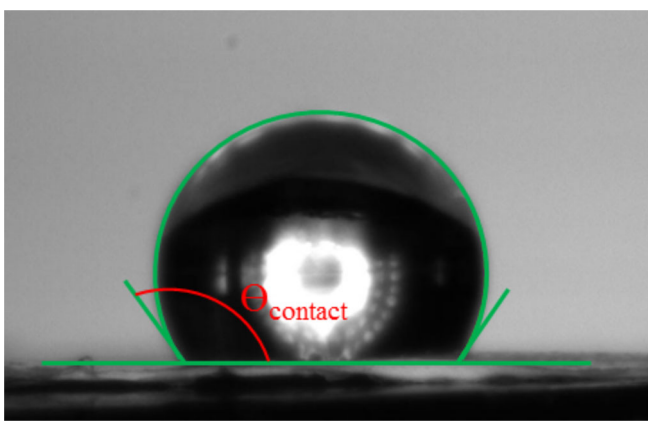

Figure 2. Contact angle measurement using the LBADSA plugin on ImageJ. [Color figure can be viewed at wileyonlinelibrary.com]

SEM of Cell Seeded Scaffolds. Cell seeded scaffolds were visualized using SEM after 6 days using a previously described osmium-based method.[8] Briefly, the cell seeded scaffolds were fixed overnight in 4% glutaraldehyde overnight before being incubated in 0.1% osmium for 30 min followed by dehydration in ethanol and hexamethyldisilazane. Scaffolds were then sputter coated and visualized as per Scanning Electron Microscopy section above. Scaffold confluency was estimated during the imaging process. The representative SEM images shown in Figure 4(e) were taken to best represent the confluency found across the whole scaffold. Confluency was measured using ImageJ (NIH) software. Briefly, SEM images were thresholded to differentiate between the scaffold and the cells. Total area coverage was then measured and converted into a percentage confluency.

CellTiter-Blue Cell Viability Assay

The assay was performed at 3 and 6 days as per manufacturer's instructions (Promega). Briefly, cell seeded scaffolds were removed and placed in new wells (48-well plate). Each well was topped up with 300 µL of media and 75 µL of CellTiter-Blue assay (4:1 ratio). The plate was lightly shaken for 1 min and then wrapped in tinfoil and incubated for 3.5 h. After incubation, 100 µL samples (×3) of the media/assay were taken from each scaffold and pipetted into a black well plate. The plate was measured in a Modulus II microplate reader at ex: 525 nm and em: 580–640 nm. For each condition group, $n = 4$.

DNA Quantification

Native and decellularized samples were frozen and lyophilized before being incubated in a papain digestion solution containing 2.5 U of papain, 5 m*M* cysteine HCL, and 5 m*M* *Ethylenediaminetetraacetic acid* (ETDA) in DNA-free water at 60 °C for 24 h (all reagents from Sigma-Aldrich, U.K.). Total DNA content was measured using a Quant-iTTMPicoGreen assay kit (ThermoFisher, U.K.) as per the manufacturers' instructions, $n = 4$.

Fourier Transform Infrared Spectroscopy

Fourier transform infrared spectroscopy (FTIR) was used to confirm the successful inclusion of ECM into the electrospun PCL fibers. FTIR spectra were recorded using a Nicolet iS10 spectrometer with a Smart iTX diamond attenuated total reflection detector (all from Thermo Fisher Scientific), in the wave range of 400–4000 per cm at a resolution of 1 per cm using OMNIC Spectra software (Thermo Fisher Scientific), $n = 5$.

Statistical Analysis

Data were expressed as mean ± 1 standard deviation. Statistical analysis was performed using one-way analysis of variance with *post hoc* Fisher test.

RESULTS

Decellularization

Bovine aorta was successfully decellularized using a 0.5% SDS perfusion treatment. Relative DNA content was measured using a Quant-iT PicoGreen assay kit (ThermoFisher) and dropped 96.5% as shown in Figure 3. Furthermore, H&E staining shows that the nuclear content of the aorta has been successfully removed [Figure 3(b, c)].

Scaffold Structure

All three scaffolds were successfully electrospun using the same parameters (Figure 4). This leads to three scaffolds with very similar architectures. No significant differences in average fiber diameter were noted across the three scaffolds, with diameters ranging from 0.90 ± 0.19 μm for the 1% aorta ECM scaffold to 0.97 ± 0.19 μm for the PCL-only scaffold (Figure 4). Similarly, the fiber orientations for all three scaffolds was very similar, with normalized frequency of fiber orientation peaking at an angle of 45° for all three scaffolds (Figure 4).

Fourier Transform Infrared Spectroscopy

The FTIR results showed that the aorta ECM was successfully incorporated into the electrospun fibers at both concentrations. Spectra were taken for the PCL fibers alone, both PCL/ECM concentrations fibers and the decellularized ECM. Characteristic peaks from the PCL and the ECM were found in both ECM/PCL scaffolds suggesting that the ECM had been incorporated into the PCL fibers. As expected, ECM peaks were more pronounced in the 1% ECM scaffolds than the 0.25% ECM scaffold which suggests that a higher quantity of ECM had been incorporated into the PCL fibers. Figure 5(a) shows peaks at 1705–1715, 1650–1660, and 1535–1545 per cm, which can be attributed to the carboxyl group in the PCL, the amide I group in the ECM, and the amide II group in the ECM, respectively.[21–23]

Mechanical Testing

Tensile Testing. Tensile testing was performed using an Instron tensile tester and showed significant differences in how each scaffold performed mechanically. All scaffolds were stretched until failure. The PCL scaffold had the highest Young's modulus in the 0–5% strain range (19.2 ± 1.7 MPa), followed by the 0.25% aorta ECM scaffold (16.1 ± 1.9 MPa) and then 1% aorta ECM scaffold (13.5 ± 0.7 MPa) [Figure 5(c)]. The Young's modulus for each scaffold dropped at each subsequent strain band, with the trend of lower stiffness for higher ECM concentration reversing in the 15–20% strain band. This phenomena can be seen in the stress versus strain curve [Figure 5(b)], where after approximately 20% strain, the PCL scaffold becomes very plastic (shallow gradient) and the 1% aorta ECM scaffold remains somewhat elastic (steeper gradient), with the 0.25% aorta ECM scaffold having a gradient between the two other scaffolds. This suggests that the incorporation of ECM is directly related to this increase in scaffold elasticity into the higher strain range.

It was also noted during tensile testing that the higher ECM concentrations lead to lower failure strains. The 1% aorta ECM and 0.25% aorta ECM scaffolds had failure strains 47% ($p > 0.001$)

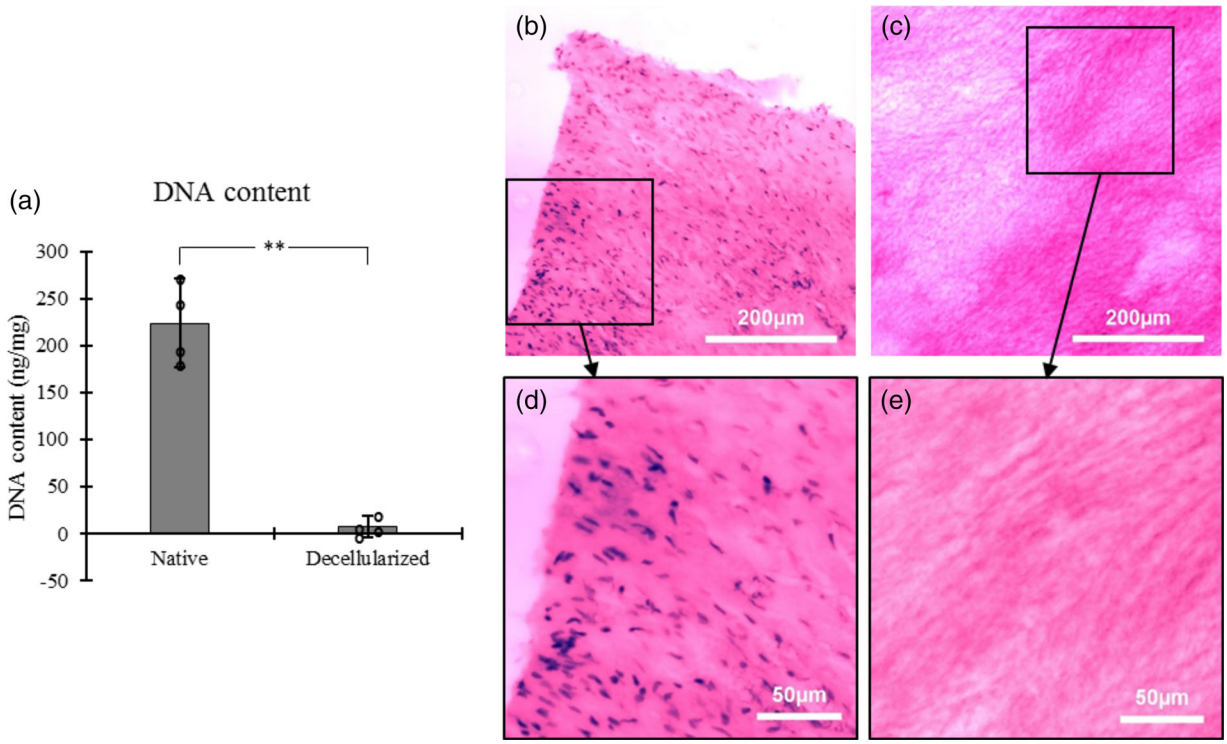

Figure 3. (a) DNA content of aorta before and after decellularization. (b, d) The aorta before decellularization. (c, e) The aorta after decellularization. [Color figure can be viewed at wileyonlinelibrary.com]

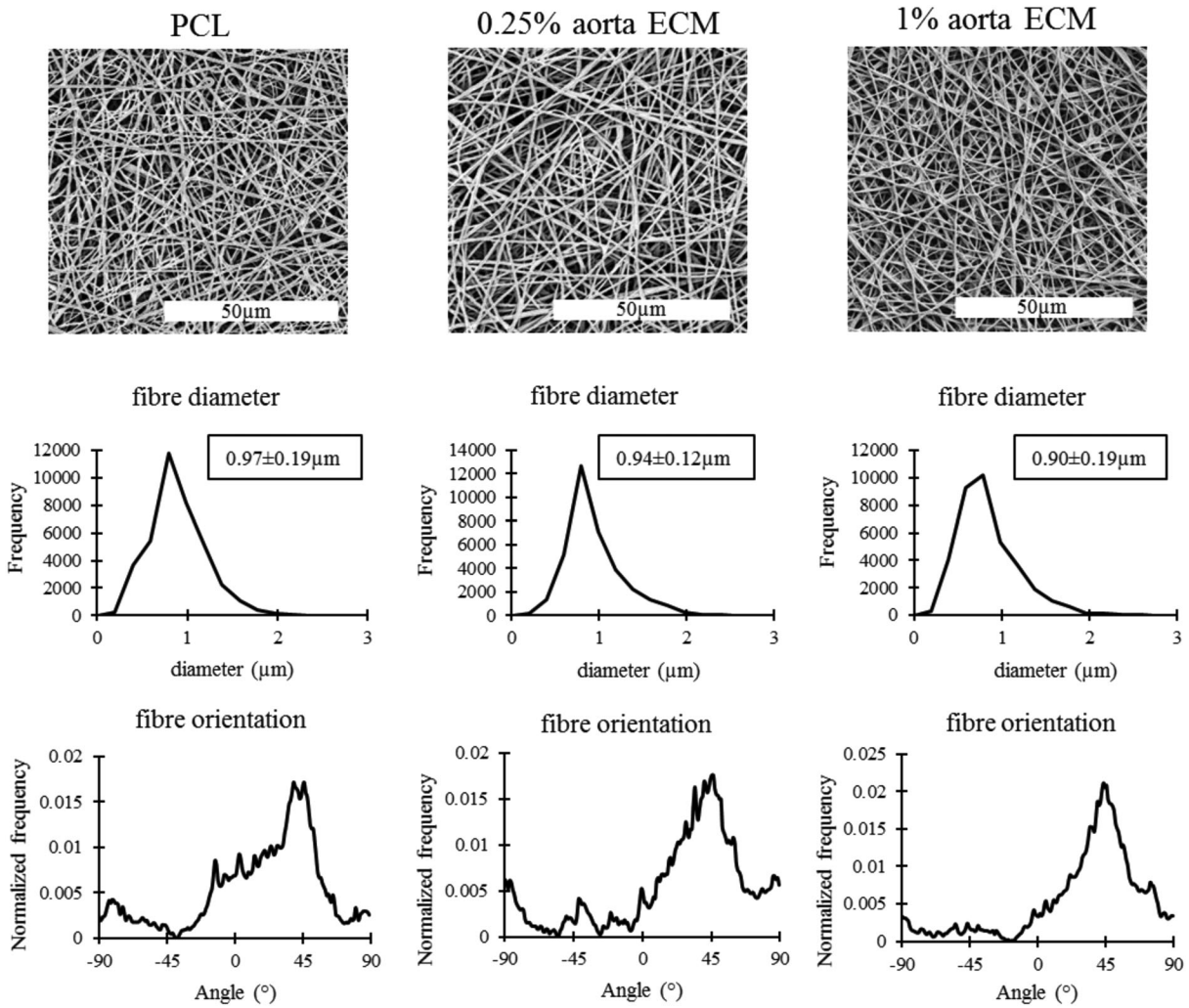

Figure 4. (a) SEM images of the three electrospun scaffolds. (b) Fiber diameter distribution of all three scaffolds. (c) Fiber orientation distribution of all three scaffolds.

and 2.6% (no significance [ns]) lower than the PCL-only scaffold, respectively. Likewise, the ultimate tensile strength of the scaffolds increased by 84.3% ($p > 0.001$) and 77.9% ($p > 0.001$) for 1% aorta ECM and 0.25% aorta ECM compared to the PCL-only scaffold, respectively.

Compliance Measurements. Values for compliance were calculated based on eq. (2). Compliance was seen to increase with ECM concentration—the 0.25% ECM and 1% ECM scaffolds had compliance values 19% ($p > 0.05$) and 42% ($p > 0.01$) larger than the PCL-only scaffold. Results shown in Table I.

Contact Angle Measurement

Contact angle measurements showed how incorporating aorta ECM into the scaffold drastically increased the hydrophilicity of the scaffold (Table I). After 0.2 s (first image after contact), the 1% aorta ECM and 0.25% aorta ECM scaffolds had contact angles 31.1% (ns) and 21.8% (ns) lower than the PCL-only scaffold. This drop in contact angle was even bigger after 5 s, where the 1% aorta ECM and 0.25% aorta ECM scaffolds had contact angles 77.5% ($p > 0.01$) and 30.3% (ns) lower than the PCL-only scaffold.

Cellular Testing/Visualization

Cell Viability. Cell viability results showed no significant differences between the three scaffolds and no change in viability between the two time points [Figure 5(d).

Scanning Electron Microscopy. SEM images show a functional HUVEC monolayer after 6 days of culture on all three scaffolds [Figure 5(e). Furthermore, the three scaffolds showed confluences ranging from 68 to 81%, and all three scaffolds appear to show HUVECs with very similar morphologies. These results validate the cell viability results, suggesting that all three scaffolds were capable of accommodating a healthy layer of HUVECs.

DISCUSSION

Electrospun polymer scaffolds have regularly been used in tissue engineering as platforms for vascular tissue regeneration.[24] Electrospinning generates fibrous scaffolds with a high degree of

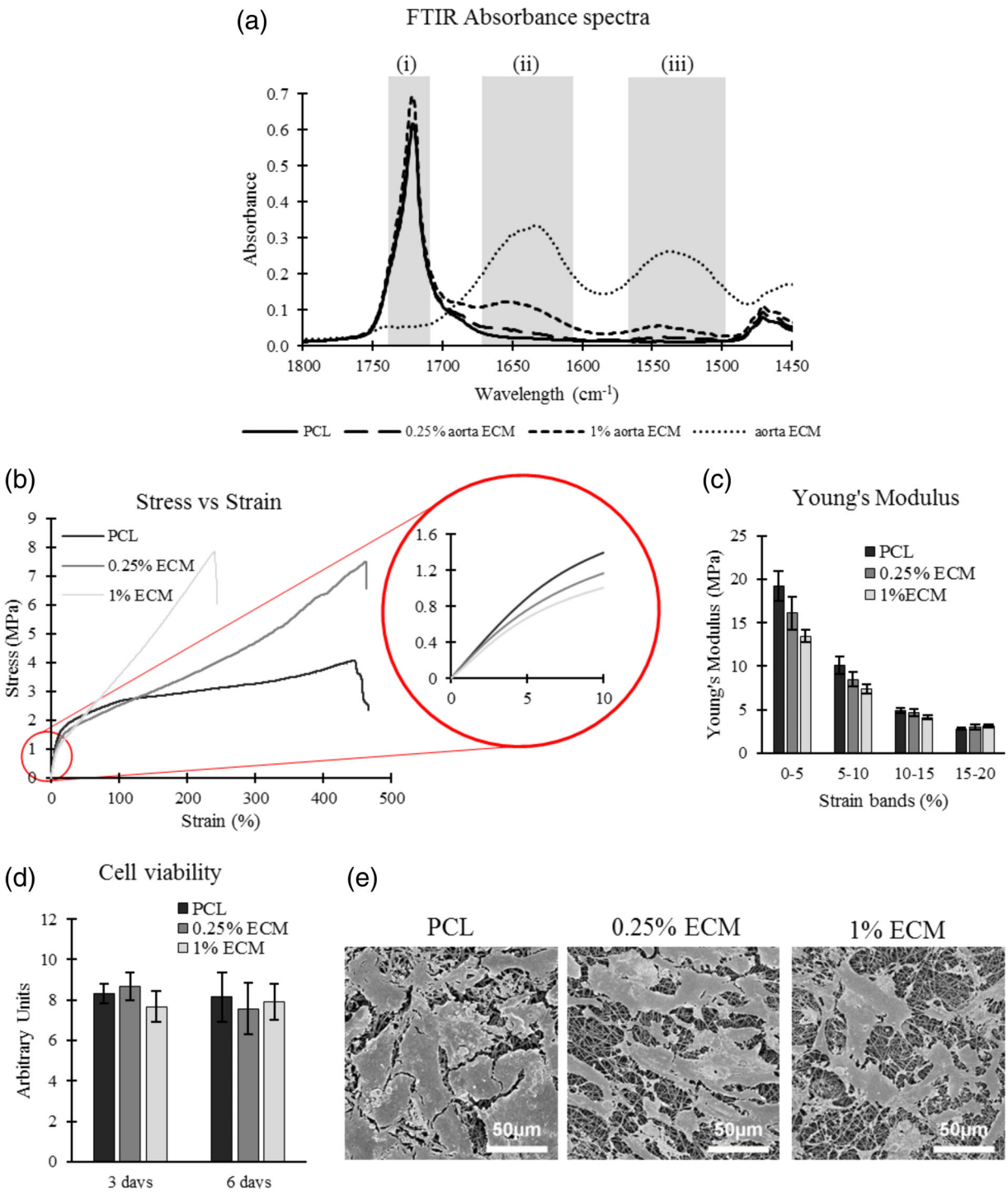

Figure 5. (a) Representative FTIR curves showing the inclusion of ECM into the PCL fibers. Peaks for (i) carbonyl group, (ii) amide I group, and (iii) amide II group are highlighted. (b) Representative stress versus strain for the three scaffolds. (c) Young's modulus of all three scaffolds at different strain bands, $n = 6$. (d) Cell viability of HUVECs on all three scaffolds after 3 and 6 days, $n = 4$. (e) Representative SEM images of HUVEC monolayer on all three scaffolds after 6 days. [Color figure can be viewed at wileyonlinelibrary.com]

architectural and mechanical repeatability.[17,24] In this study, we have used PCL, a commonly used polymer for electrospinning tissue engineering application.[5,10] We were able to spin three extremely similar scaffolds using the same parameters, which demonstrates the repeatable properties that electrospinning PCL possess. Furthermore, we noted that the inclusion of ECM had very little effect on how the solution spun, with fiber diameter being similar for all three scaffolds (0.90, 0.94, and 0.97 μm). By having three similar morphologies (fiber diameter and fiber orientation, as seen in Figure 3), we have ensured that the only

Table I. Mechanical Properties of Scaffolds

	PCL	0.25% ECM	1% ECM
Ultimate tensile strength (MPa)	4.26 ± 0.33	7.58 ± 1.59	7.85 ± 1.03
Failure strain (%)	464 ± 40	452 ± 59	244 ± 29
Compliance (mL/mmHg)	0.049 ± 0.004	0.059 ± 0.006	0.070 ± 0.004
Contact angle after 0.2 s (°)	114.4 ± 8.9	89.5 ± 37.7	75.4 ± 25.6
Contact angle after 5 s (°)	98.7 ± 25.2	68.8 ± 43.6	22.2 ± 10.5

difference between the three scaffolds is the PCL:ECM ratio within the fibers (100:0, ~97:3, and ~ 88:12), meaning that the PCL:ECM ratio of the scaffold can be one of the factors attributed to the differences in mechanical properties and cellular performance.

FTIR results [Figure 5(a) showed that the decellularized ECM had been successfully incorporated into the PCL scaffolds. Peaks at the amide I and amide II bonds (two characteristic bonds found in ECM proteins) can be seen in both PCL/ECM scaffolds, showing that the ECM had been incorporated into the scaffold.[22,23] Interestingly, as the ECM concentration increased, the peak at these two Amide bonds also increased, suggesting that increasing ECM concentration did lead to more ECM being incorporated into the PCL fibers. All three scaffolds showed peaks at the carboxyl group, which can be attributed to the PCL.[21] FTIR is a surface characterizing method that has been shown to measure to depths of 5 μm[25]—the fibers in this study are all under 1 μm thick, suggesting that a full characteristic profile of the fiber is being achieved through FTIR.

Tensile testing leads to some interesting results that demonstrate the effect of including ECM into the electrospun fibers. We noted that the 1% ECM scaffold had a lower stiffness than the PCL-only scaffold. This result can possibly be explained by aortic arch ECM (the ECM used in this study), comprising of approximately 40% elastin and 20% collagen.[26] Elastin has been shown to have a half-life of around 74 years. As people age, the quantity of elastin in their aortas decreases, which leads to a very large increase in aortic stiffness—a 394% increase in stiffness was noted between the ages of 25 and 70.[27,28] This suggests that a lower quantity of elastin in the scaffold would lead to a higher stiffness and lower compliance.

Furthermore, including aortic ECM resulted in a drastic reduction in failure strain, as seen in Table I. This can possibly be explained by collagen having a failure strain of 13% and elastin between 100 and 150%,[29] compared to the PCL-only scaffold having a failure strain of 464% (our results). Hence, a fiber made up of a ~88:12 PCL to ECM ratio (1% ECM) would be expected to fail at a lower strain than the fiber with a 100:0 PCL to ECM ratio (PCL only). Additionally, most cells feel and respond to the stiffness of their substrate/environment, therefore being able to tailor scaffold stiffness has benefits for tissue engineering.[30]

Water droplet contact angle is defined as the angle formed at the intersection of the liquid–solid interface—the lower this angle is, the more hydrophilic the solid is.[31] Studies have shown that altering the contact angle of a scaffold can have effects on cell adhesion.[5,32] Furthermore, the addition of ECM to an electrospun polymer scaffold has been shown to reduce water contact angle.[5] This result was noted in our study, with a 31.1 and 77.5% lower contact angle in the 1% ECM scaffold compared to the PCL-only scaffold for the 0.2 s measurement and 5 s measurement, respectively. After 0.2 s, the PCL-only scaffolds had a contact angle of 114.4° (hydrophobic[32]), compared to 75.4° for the 1% ECM scaffold.

Cellular testing and visualization showed that the HUVECs reacted similarly to all three scaffolds. Cell viability [Figure 5(d) showed no significant differences between the three scaffolds over both time points, suggesting that including ECM had no impact on their proliferation. Similarly, SEM images [Figure 5(e) show that the HUVECs had similar morphologies on all three scaffolds. Further work looking into gene analysis is required to gain a full bioactivity profile for these scaffolds.

Sterilization in this study was achieved using 70% ethanol, which is sufficient for preliminary *in vitro* studies but is not a clinically translatable method of terminal sterilization. Studies have shown that some methods of terminal sterilization do have detrimental effects on the structure, mechanical integrity, and cell hosting abilities of decellularized ECM.[33,34] The majority of currently marketed biological devices that use decellularized ECMs are terminally sterilized using gamma irradiation, ethylene oxide, or electron beam processing, which shows that decellularized ECMs can be efficiently sterilized before being translated to the clinic.[35] Furthermore, peracetic acid as a terminal sterilization method has been shown to have no effect on the structure or mechanical strength of ECM, while also maintaining its ability to host cells.[33] Therefore, translating this work to a clinical setting where an approved terminal sterilization method is required would rely on one of the aforementioned sterilization methods.

Although a relatively hydrophilic contact angle of approximately 60° has been shown to lead to higher cell adhesion,[32] this could also have problematic effects and leads to the binding of unwanted cells, proteins, and growth factors. It has been shown that blood-contacting devices and tissue engineering substrates require an appropriate balance of hydrophilic and hydrophobic entities.[36] Therefore, with the final goal for vascular tissue engineering strategies often being *in vivo* implantation, it is very important to consider the fact that the scaffold will be in contact with a variety of constituents that you may not want binding to the scaffold. Hence, in certain situations, higher hydrophobicity may be desirable to reduce the binding of unwanted substances. This applies for approaches such as bypass grafting where local cell attachment to the implant is unwanted. Therefore, being able to control the hydrophobicity of the scaffold/implant is desirable.

CONCLUSIONS

In this study, we successfully combine aortic ECM with PCL and electrospun randomly aligned nanofiber scaffolds. We noted that including ECM reduced stiffness and increased compliance at lower strains and increased the elasticity of the nanofibers beyond its yield strength. Furthermore, the inclusion of ECM reduced the failure strain and increased the ultimate tensile strength of the scaffold. Additionally, including ECM into the scaffold had the effect of reducing the water droplet contact angle. Future work should focus on quantifying the elastin and collagen in the ECM and/or scaffold to validate any theorem regarding these ECM proteins altering the mechanical and physical properties of the scaffold.

Our findings show that the mechanical properties of electrospun scaffolds can be changed through the addition of ECM. By altering the polymer to ECM ratio, a wide array of mechanical properties can be achieved, allowing for tissue-specific tailoring of scaffolds.

ACKNOWLEDGMENTS

The authors would like to thanks Alistair Elfick for use of lab facilities (Institute of Bioengineering, the University of Edinburgh) and Steve Mitchell for imaging assistance (BioSEM). This work was funded by an Engineering & Physical Sciences Research Council (ESPRC) doctoral training partnership studentship EP/N509644/1 and a UK Regenerative Medicine Platform II grant MR/L022974/1.

REFERENCES

1. Wilkins, E.; Wilson, L.; Wickramasinghe, K.; Bhatnagar, P.; Leal, J.; Luengo-Fernandez, R.; Burns, R.; Rayner, M.; Townsend, N. European Cardiovascular Disease Statistics; European Heart Network: Brussels, Belgium, **2017**.
2. Hartman, O.; Zhang, C.; Adams, E. L.; Farach-Carson, M. C.; Petrelli, N. J.; Chase, B. D.; Rabolt, J. F. *Biomaterials*. **2011**, *31*, 5700.
3. Han, J.; Gerstenhaber, J. A.; Lazarovici, P.; Lelkes, P. I. *Biomacromolecules*. **2013**, *14*, 1338.
4. Ott, H. C.; Matthiesen, T. S.; Goh, S. K.; Black, L. D.; Kren, S. M.; Netoff, T. I.; Taylor, D. A. *Nat. Med.* **2008**, *14*, 213.
5. Gao, S.; Guo, W.; Chen, M.; Yuan, Z.; Wang, M.; Zhang, Y.; Liu, S.; Xi, T.; Guo, Q. *J. Mater. Chem. B*. **2017**, *5*, 2273.
6. Garrigues, N. W.; Little, D.; Sanches-Adams, J.; Ruch, D. S.; Guilak, F. *J. Biomed. Mater. Res. Part A*. **2014**, *102*, 3998.
7. Kim, T. H.; Jung, Y.; Kim, S. H. *Tissue Eng. Part A*. **2018**, *24*, 830.
8. Grant, R.; Hay, D. C.; Callanan, A. *Tissue Eng. Part A*. **2017**, *23*, 650.
9. Agarwal, S.; Wendorff, J. H.; Greiner, A. *Polymer (Guildf)*. **2008**, *49*, 5603.
10. Burton, T. P.; Corcoran, A.; Callanan, A. *Biomed. Mater.* **2017**, *13*, 015006.
11. Schoen, B.; Avrahami, R.; Baruch, L.; Efraim, Y.; Goldfracht, I.; Elul, O.; Davidov, T.; Gepstein, L.; Zussman, E.; Machluf, M. *Adv. Funct. Mater.* **2017**, *27*, 1.
12. Chakrapani, V. Y.; Gnanamani, A.; Giridev, V. R.; Madhusoothanan, M.; Sekaran, G. *J. Appl. Polym. Sci.* **2012**, *125*, 3221.
13. Grant, R.; Hallett, J.; Forbes, S.; Hay, D.; Callanan, A. *Sci. Rep*. **2019**, *9*, 1.
14. Hotaling, N. A.; Bharti, K.; Kriel, H.; Simon, C. G., Jr. *Biomaterials*. **2015**, *61*, 327.
15. Munir, N.; Callanan, A. *Biomed. Mater.* **2018**, *13*, 051001.
16. Dunphy, S.; Reid, J. A.; Burton, T. P.; Callanan, A. *Biomed. Phys. Eng. Express.* **2018**, *4*, 057004.
17. Burton, T. P.; Callanan, A. *J. Tissue Eng. Regen. Med.* **2018**, *15*, 301.
18. Callanan, A.; Davis, N. F.; Walsh, M. T.; McGloughlin, T. M. *Med. Eng. Phys.* **2012**, *34*, 1368.
19. Callanan, A.; Davis, N. F.; McGloughlin, T. M.; Walsh, M. T. *J. Biomech.* **2014**, *47*, 1885.
20. Stalder, A. F.; Melchior, T.; Müller, M.; Sage, D.; Blu, T.; Unser, M. *Colloids Surf. A Physicochem. Eng. Asp.* **2010**, *364*, 72.
21. Elzein, T.; Nasser-Eddine, M.; Delaite, C.; Bistac, S.; Dumas, P. *J. Colloid Interface Sci.* **2004**, *273*, 381.
22. Camacho, N. P.; West, P.; Torzilli, P. A.; Mendelsohn, R. *Biopolymers*. **2001**, *62*, 1.
23. Garidel, P.; Schott, H. *BioProcess Tech.* **2006**, *1*, 48.
24. Karaman, O.; Şen, M.; Demirci, E. A. In Electrospun Materials for Tissue Engineering and Biomedical Applications: Research, Design and Commercialization; Woodhead Publishing: Sawston, Cambridge, **2017**. p. 261.
25. Kazarian, S. G.; Chan, K. L. A. *Analyst*. **2013**, *138*, 1940.
26. Grant, R. A. *J. Atheroscler. Res.* **1966**, *7*, 463.
27. Astrand, H.; Stalhand, J.; Karlsson, J.; Karlsson, M.; Sonesson, B.; Lanne, T. *J. Appl. Physiol.* **2011**, *110*, 176.
28. Shapiro, S. D.; Endicott, S. K.; Province, M. A.; Pierce, J. A.; Campbell, E. J. *J. Clin. Invest.* **1991**, *87*, 1828.
29. Muiznieks, L. D.; Keeley, F. W. *Biochim. Biophys. Acta*. **2013**, *1832*, 866.
30. Discher, D. E. *Science*. **2005**, *310*, 1139.
31. Bracco, G.; Holst, B. In Surface Science Techniques; Yuan, Y.; Lee, T., Eds.; Springer: Berlin, Germany, **2013**; p. 3.
32. Dowling, D. P.; Miller, I. S.; Ardhaoui, M.; Gallagher, W. M. *J. Biomater. Appl.* **2011**, *26*, 327.
33. Matuska, A. M.; Mcfetridge, P. S.; Family, J. C. P. *J. Biomed. Mater. Res. B Appl. Biomater.* **2016**, *103*, 1.
34. Crapo, P. M.; Gilbert, T. W.; Badylak, S. F. *Biomaterials*. **2012**, *32*, 3233.
35. Freytes, D. O.; Badylak, S. F. In Encyclopedia of Medical Devices and Instrumentation; Webster, J. G., Ed., Wiley & Sons, Inc: Hoboken, New Jersey, United States, **2006**; p. 273.
36. Menzies, K. L.; Jones, L. *Optom. Vis. Sci.* **2010**, *87*, 387.